

# A new pillared Cd-organic framework as adsorbent of organic dyes and as precursor of CdO nanoparticles

Samira Gholamali Ghomshehzadeh<sup>a</sup>, Valiollah Nobakht<sup>a,\*</sup>, Nahid Pourreza<sup>a</sup>, Pierluigi Mercandelli<sup>b</sup>, Lucia Carlucci<sup>b</sup>

<sup>a</sup> Department of Chemistry, Faculty of Sciences, Shahid Chamran University of Ahvaz, Ahvaz, Iran

<sup>b</sup> Dipartimento di Chimica, Università degli Studi di Milano, via Camillo Golgi 19, 20133 Milano, Italy

## ARTICLE INFO

### Article history:

Received 3 May 2019

Accepted 23 November 2019

Available online 16 December 2019

### Keywords:

MOF  
Pillar ligands  
Cd(II) complex  
Congo Red  
Neutral Red  
Adsorption

## ABSTRACT

A new neutral cadmium-organic framework with a pillared layer structure,  $[\text{Cd}_3(\text{BTC})_2(4\text{-bpdb})_2]$  ( $\text{H}_3\text{BTC}$  = benzene-1,3,5-tricarboxylic acid; 4-bpdb = 1,4-bis(4-pyridyl)-2,3-diaza-1,3-butadiene), has been synthesized via solvothermal reaction of cadmium nitrate with the tricarboxylic acid  $\text{H}_3\text{BTC}$  and the linear bispyridyl linker 4-bpdb. The complex has been characterized by single crystal X-ray diffraction, showing to possess a 3D porous network of **jcr7** topology. The capability of the prepared MOF in adsorbing the organic dyes Congo Red (**CR**) and Neutral Red (**NR**), together with kinetics and thermodynamics of their adsorption, have been investigated in detail. The adsorption process was well described by pseudo-first order and pseudo-second order kinetics for **CR** and **NR**, respectively. In addition, conversion of the MOF 3D architecture into nano-sized cadmium oxide particles has also been studied.

© 2019 Elsevier Ltd. All rights reserved.

## 1. Introduction

Metal-Organic Frameworks (MOFs) are an interesting category of materials containing metal or metal-cluster nodes and multi-topic organic linkers [1]. Tunability of cluster nodes and organic linkers offers infinite possibilities to design and synthesize a variety of MOF structures with fascinating topologies and useful properties. Moreover, MOF structures obtained by self-assembly methods can undergo a wide range of chemical functionalization via post-synthetic modification (PSM) reactions [2]. The ease of tailorability combined with outstanding features, such as ultrahigh Brunauer–Emmett–Teller (BET) surface area and high thermal stability and porosity, brought these materials to the attention of many scientists in both academia and industry [3]. In order to prepare pre-designed MOFs, the best choice is to employ rigid linkers containing carboxylate or pyridyl donating groups. In particular, the combination of carboxylates with pyridyl-based linkers as pillars is an intriguing strategy to obtain designed structures. Indeed, carboxylate ligands usually form 2D-sheet structures with a highly predictable network topology by means of coordination to the metal ions. The remaining coordination sites of the metal centers are then occupied by the nitrogen atoms of the pyridyl-based

ligands to give rise to 3D structures with the desired network topology [4].

Metal-organic frameworks exhibit a wide range of properties and potential applications, including gas sorption and separation, catalysis, sensing, and biomedical applications [5]. Furthermore, results have proved that MOFs offer a promising toolbox for preparing advanced nanomaterials that are not easily obtainable using conventional methods [6]. Among metal-oxide nanoparticles (NPs), cadmium oxide is a well-known n-type semiconductor and shows applications in various fields such as optoelectronics, solar cells, transparent electrodes and gas sensors [7]. Up to now, several approaches have been developed to produce CdO nanostructures including solvothermal, sol-gel, sonochemical, precipitation, and wet chemical methods [8]. Thermal decomposition of inorganic precursors or Cd-organic coordination networks is also a valuable route to obtain CdO nanostructures with different shapes and sizes [6].

On the other hand, the presence of organic and inorganic pollutants in waters and wastewaters is a serious problem and causes worldwide concern, due to their harmful effects and potential carcinogenic hazards [9]. Significant amounts of organic dyes have been produced by textile, leather, paper, and plastic factories which should be treated before their discharging into the environment. Several approaches, such as adsorption, coagulation, ion exchange, filtration, photocatalysis, and advanced oxidation have been used to remove organic dyes from aqueous media [10].

\* Corresponding author.

E-mail address: [v.nobakht@scu.ac.ir](mailto:v.nobakht@scu.ac.ir) (V. Nobakht).

Among them, adsorption of dyes is an attractive method due to its simplicity, effectiveness, and affordability [11]. Recently, adsorption by MOFs of toxic heavy metal ions and organic pollutants from the effluents has become of great interest for researchers [12]. Zhao et al. employed several cationic indium-organic frameworks for the adsorption and separation of organic dyes through anion-exchange processes [13]. Several reports concerning the selective adsorption and separation of anionic or cationic organic dyes by positively- or negatively-charged MOFs via ion-exchange processes have been reported up to now [14]. Adsorption of organic dyes into the pores or on the surface of neutral MOFs has also been reported [15]. In this context, several mechanisms of interaction between the dye molecules and the MOF surface have been proposed [16], such as electrostatic interaction, acid–base reactions, hydrogen bonding,  $\pi \cdot \cdot \pi$  stacking, and hydrophobic interactions.

In this work, a new Cd(II) metal-organic framework with an interesting network topology has been prepared via solvothermal synthesis using a tricarboxylate linker in combination with a bis-pyridyl ligand. The efficiency of the synthesized MOF in the adsorption of some organic dyes has been studied in detail. In addition, spherical CdO nanoparticles have been obtained via calcination of the MOF at 500 °C.

## 2. Experimental

### 2.1. Materials and physical measurements

The starting materials were purchased from commercial sources and used without further purification. Infrared spectra (4000–400  $\text{cm}^{-1}$ ) were recorded as KBr discs with a BOMEN MB102 or Perkin Elmer Spectrum Two FT-IR spectrometers. Elemental analyses for C, H, and N were performed on a Thermo Finnigan Flash EA 1120 CHN analyzer. UV–Visible spectra were recorded on a GBC Cintra 1010 spectrophotometer. Particle size and morphology of CdO NPs were determined respectively by dynamic light scattering using a Qudix Inc. Scatterscope I and by scanning electron microscopy using a KYKY-EM3200e. Powder X-ray diffraction (PXRD) patterns were recorded on a Philips X'Pert Pro diffractometer (Cu  $K\alpha$  radiation,  $\lambda = 1.54184 \text{ \AA}$ ) in the 5–50°/90° 2 $\theta$  range. The PXRD pattern was simulated on the base of single-crystal data using Mercury [17]. Topological analysis was performed using ToposPro [18].

### 2.2. Preparation of 1,4-bis(4-pyridyl)-2,3-diaza-1,3-butadiene

The ligand 1,4-bis(4-pyridyl)-2,3-diaza-1,3-butadiene (4-bpdb) was prepared according to a previously published method [19]. Typically, 0.53 mL (11 mmol) of hydrazine (80 wt% solution in water) was added dropwise to a solution of 4-pyridinecarboxaldehyde (2.1 mL, 22 mmol) in ethanol (15 mL). Two drops of formic acid were added and the mixture was stirred at room temperature for 24 h. The yellow solid was filtered, washed several times with ethanol and diethyl ether (2 × 5 mL), and dried in air (yield: 86%).

### 2.3. Synthesis of $[\text{Cd}_3(\text{BTC})_2(4\text{-bpdb})_2]$ (Cd-MOF)

$\text{Cd}(\text{NO}_3)_2 \cdot 4\text{H}_2\text{O}$  (0.102 g, 0.33 mmol), benzene-1,3,5-tricarboxylic acid ( $\text{H}_3\text{BTC}$ , 0.046 g, 0.22 mmol), and 1,4-bis(4-pyridyl)-2,3-diaza-1,3-butadiene (4-bpdb, 0.046 g, 0.22 mmol) were dissolved in 7 mL DMF in three separate test tubes.

The three solutions were warmed at 80 °C for 10 min. Then the solution of 4-bpdb was added to that of  $\text{Cd}(\text{NO}_3)_2 \cdot 4\text{H}_2\text{O}$  and, after stirring for 10 min, also that of  $\text{H}_3\text{BTC}$  was added to the mixture. The resulting yellowish solution was placed in a teflon-lined stainless steel autoclave and heated at 90 °C for 72 h. The mixture was

gradually cooled to room temperature over 24 h. Yellow needle-shaped single crystals of  $[\text{Cd}_3(\text{BTC})_2(4\text{-bpdb})_2]$  suitable for single crystal X-ray diffraction analysis were obtained, collected by filtration, and dried in air (0.18 g, yield: 48% based on Cd). Elemental analysis (%) calc. for  $\text{C}_{51}\text{H}_{47}\text{Cd}_3\text{N}_{11}\text{O}_{15}$ : C 44.03, H 3.41, N 11.07; found: C 44.16, H 3.30, N 11.09.

### 2.4. Adsorption experiments for Congo Red and Neutral Red

Before dye adsorption experiments, to increase the surface area of the adsorbent, crystals of Cd-MOF were ground in an agate mortar. The adsorption experiments were carried out by adding 5 mg of the adsorbent powder into a 100 mL beaker containing 20 mL of the dye solution (CR or NR) at different initial concentrations. The mixture was left under stirring for 80 min (CR) and 95 min (NR) to allow to reach the equilibrium. The solution was then transferred to a tube and centrifuged at 4000 rpm for 5 min. The supernatant solution was removed and the absorbance was measured at 499 nm and 526 nm for CR and NR, respectively. The equilibrium concentration of the dyes was determined spectrophotometrically using a calibration plot for each dye ( $A = 0.0278C + 0.0520$  and  $A = 0.0533C + 0.2533$  for CR and NR, respectively). The amount of adsorbed dye at time  $t$  was calculated using the following equation:  $q_t = (C_0 - C_t)V/m$ , where  $q_t$  is the adsorption capacity,  $C_0$  and  $C_t$  are the initial and the equilibrium concentration of the dye,  $V$  is the volume of the sample solution and  $m$  is the mass of the adsorbent.

### 2.5. Synthesis of CdO nanoparticles

Cd-MOF (0.207 g) was transferred into a 25 mL crucible and heated at 500 °C for 5 h. Upon gradual cooling, red-brown nanoparticles of CdO were obtained, collected (0.05 g, yield: 72%), and characterized by FT-IR spectroscopy, PXRD analysis, particle size analysis, and scanning electron microscopy.

### 2.6. Single crystal X-ray diffraction analysis

A full-sphere dataset was collected at 150(2) K on a Bruker Apex II diffractometer using graphite-monochromatized Mo  $K\alpha$  radiation ( $\lambda = 0.71073 \text{ \AA}$ ), operating in  $\omega$ -scan mode. Even if the reflections could be indexed with a monoclinic unit cell, a careful inspection of the diffraction spots in the reciprocal space and a subsequent analysis with CELL\_NOW [20] showed that the crystal was a non-merohedral twin composed of two triclinic domains of comparable dimensions (the twin operator being a 180° rotation about  $b^*$ ). All attempts to isolate a non-twinning specimen, changing also the crystallization conditions, were unsuccessful. The frames has been integrated refining a single triclinic unit cell and two orientation matrices (one for each domain). A multi-scan absorption correction based on a multipolar spherical harmonic expansion of equivalent intensities was applied to all data using TWINABS [20].

The structure was solved using direct methods and refined with a full-matrix least-squares procedure based on  $F^2$ , using all data [20]. The limited number of observed reflections, due to the partial superposition of the diffraction patterns of the two domains and to the overall low quality of the crystal, did not allow a free anisotropic refinement of the structure. To overcome the problem, some restraints on the atomic displacement parameters have been employed (ISOR, RIGU, and SIMU). In addition, the three dimethylformamide solvate molecules were restrained to have a similar geometry (SAME) and were refined isotropically, with a common atomic displacement parameter. Hydrogen atoms were placed at geometrically calculated positions and refined riding on their parent carbon atoms.

**Table 1**  
Crystallographic data and structure refinement details for **Cd-MOF-3DMF**.

Cd-MOF-3DMF	
Formula	C <sub>42</sub> H <sub>26</sub> Cd <sub>3</sub> N <sub>8</sub> O <sub>12</sub> ·3(C <sub>3</sub> H <sub>7</sub> NO) = C <sub>51</sub> H <sub>47</sub> Cd <sub>3</sub> N <sub>11</sub> O <sub>15</sub>
Formula mass	1391.19
T (K)	150(2)
Crystal system	triclinic
Space group	<i>P</i> -1
<i>a</i> (Å)	10.2682(9)
<i>b</i> (Å)	15.9251(14)
<i>c</i> (Å)	17.0692(15)
$\alpha$ (°)	85.187(1)
$\beta$ (°)	77.217(1)
$\gamma$ (°)	85.961(1)
<i>V</i> (Å <sup>3</sup> )	2708.5(4)
<i>Z</i>	2
<i>D</i> <sub>calcd</sub> (g cm <sup>-3</sup> )	1.706
No. of reflns collected	17,661
No. of independent reflns	9129
No. of observed reflns	4971
<i>R</i> <sub>int</sub>	0.0665
( <i>sin</i> $\theta$ / $\lambda$ ) <sub>max</sub> (Å <sup>-1</sup> )	0.841
Data/restraints/params	9129/1326/560
<i>S</i> (all data)	0.919
<i>R</i> <sub>1</sub> [ <i>I</i> > 2 $\sigma$ ( <i>I</i> )]	0.0631
<i>wR</i> <sub>2</sub> (all data)	0.1641

Crystal data and details of structure refinement are listed in Table 1, while relevant geometrical parameters describing the coordination environment of the three independent cadmium atoms are listed in Table S1.

### 3. Results and discussion

#### 3.1. Synthesis of [Cd<sub>3</sub>(BTC)<sub>2</sub>(4-bpdb)<sub>2</sub>]

Metal-organic coordination networks containing linear bis(pyridyl) pillars and multi-carboxylate ligands show a variety of structures and network topologies, which are strongly influenced by the geometry of the multi-carboxylate linkers and the coordination geometry of the metal centers. In particular, self-assembly of the 4-bpdb pillar ligand with linear or V-shaped benzenedicarboxylate linkers (1,4-BDC and 1,3-BDC, respectively) afforded 3D MOFs with **pcu** topology [4a,b] or more varied topologies [4d,21], respectively.

In this work, we use the 1,3,5-benzentricarboxylate ligand as a planar 3-connected linker and the 4-bpdb ligand as a long bis(pyridyl) pillar in presence of large Cd(II) ions to generate a MOF containing metal centers with high coordination numbers. Solvothermal reaction of Cd(NO<sub>3</sub>)<sub>2</sub>·4H<sub>2</sub>O, 4-bpdb, and H<sub>3</sub>BTC in a 3:2:2 M ratio was carried out at 90 °C in DMF obtaining single crystals of **Cd-MOF** of formula [Cd<sub>3</sub>(BTC)<sub>2</sub>(4-bpdb)<sub>2</sub>].

The new species has also been prepared as a bulk by applying more quantities of starting materials in order to obtain a sufficient amount of microcrystalline material to be employed in the subsequently described dye adsorption and CdO nanoparticles preparation experiments. The purity of the obtained bulk material has been checked by comparing its experimental PXRD spectrum with the spectrum simulated on the basis of single-crystal data (Fig. 1).

#### 3.2. Crystal structure and characterization of [Cd<sub>3</sub>(BTC)<sub>2</sub>(4-bpdb)<sub>2</sub>]

The compound crystallizes as a twin in the triclinic space group *P*-1 with *Z* = 2 (Table 1) and shows an open 3D framework architecture. The asymmetric unit contains three crystallographically independent Cd(II) ions, two BTC<sup>3-</sup> anions and two 4-bpdb molecules (Fig. 2a). Three solvate dimethylformamide molecules are also present in the asymmetric unit. Cd1 and Cd2 have a distorted pentagonal bipyramidal geometry, being coordinated to five oxy-

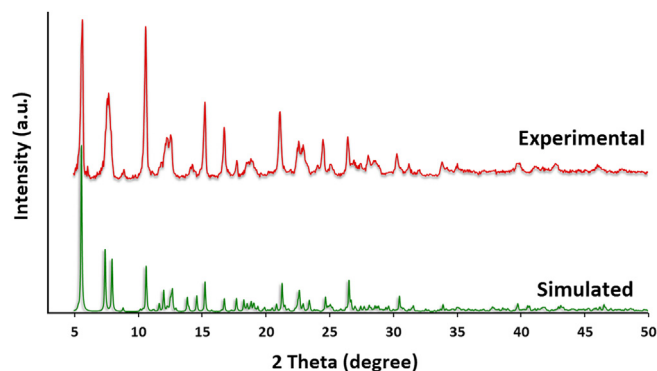


**Fig. 1.** Experimental (red) and simulated (green, from single-crystal data) powder X-ray diffraction patterns. (For interpretation of the references to colour in this figure legend, the reader is referred to the web version of this article.)

gen atoms of three distinct BTC<sup>3-</sup> ligands in the equatorial positions (Cd—O in the range 2.292(6)–2.660(6) Å) and two nitrogen atoms of two symmetry-related 4-bpdb molecules in the axial positions (Cd—N in the range 2.291(8)–2.306(8) Å). The chelating-bridging coordination mode adopted by the two BTC<sup>3-</sup> ligands about Cd1 and Cd2 gives rise to dimeric “[CdBTC]<sub>2</sub>” units characterized by a Cd...Cd distance of 3.8163(10) Å (see Figs. 2a and S1a). The third independent metal atom Cd3 is connected to three “[CdBTC]<sub>2</sub>” dimeric units by four distinct BTC<sup>3-</sup> ligands, leading to a CdO<sub>6</sub> coordination environment with a distorted trigonal-prismatic geometry (Cd—O in the range 2.294(7)–2.382(7) Å).

Fully deprotonated BTC<sup>3-</sup> ligands act as  $\mu_5$ -bridging groups via two chelating-bridging carboxylate moieties and one chelating carboxylate moiety (2.21 and 1.11 according to the Harris notation [22], respectively) (Fig. S1a).

Extended connection of Cd(II) centers by the BTC<sup>3-</sup> linkers in the *ac* plane forms a wavy thick layer with a thickness of about 5.7 Å (Fig. S1c). Along the *b* direction these thick layers are pillared by bridging 4-bpdb ligands which, connecting Cd1 and Cd2 atoms belonging to adjacent layers, give the single 3D framework (Fig. 2b,c). The N...N distance along the bridging *trans*-4-bpdb ligands is 11.4 Å, while the pillaring distance, defined as the Cd—N...N—Cd separation, is 15.9 Å. In order to have a better insight into the complex 3D structure, a topological analysis was also performed. Simplification of the structure by the program ToposPro [18] gives a (4-c)(5-c)<sub>2</sub>(5-c)<sub>2</sub>-connected network with point symbol (4<sup>2</sup>.6<sup>7</sup>.8)<sub>2</sub>(4<sup>3</sup>.6<sup>2</sup>.8)(4<sup>5</sup>.6<sup>4</sup>.8)<sub>2</sub>. In this network description the 4-c node coincides with Cd3 atoms, one of the two 5-c nodes coincides with Cd1 and Cd2 atoms while the other lies on the BTC<sup>3-</sup> ligands. Moreover, this 3D network can be seen as derived from a (3-c)<sub>2</sub>(4-c)(5-c) 2D network with point symbol (4<sup>2</sup>.6)<sub>2</sub>(4<sup>3</sup>.6<sup>2</sup>.8)(4<sup>5</sup>.6<sup>4</sup>.8)<sub>2</sub> that, by pillaring, transforms Cd1 and Cd2 atoms from 3-c to 5-c nodes and the 2D thick layers to a 3D framework (Fig. 2b,c). The topological type for this 3D net is **jc7**, as reported in the database of ToposPro (personal.ttd). Interestingly, this is the second example of a coordination polymer with **jc7** topology. The other crystal structure showing this topology is strictly related to the present species being an isostructural pillared MOF in which the only difference can be found in the bispyridyl ligand, namely [Cd<sub>3</sub>(BTC)<sub>2</sub>(pbptz)<sub>2</sub>] (pbptz = 3,6-bis(4-pyridyl)-1,2,4,5-tetrazine) [23]. The presence of different pillars leads to slightly different N...N and Cd...Cd distances (11.2 and 15.8 Å vs 11.4 and 15.9 Å in [Cd<sub>3</sub>(BTC)<sub>2</sub>(pbptz)<sub>2</sub>] and in the present structure, respectively). A more evident difference concerns the thickness of the [Cd<sub>3</sub>(BTC)<sub>2</sub>] layers in the two structures (5.0 vs 5.7 Å, respectively). The increased thickness of the layer in the present structure may be attributed to a skewed orientation of the N...N vector of the 4-bpdb

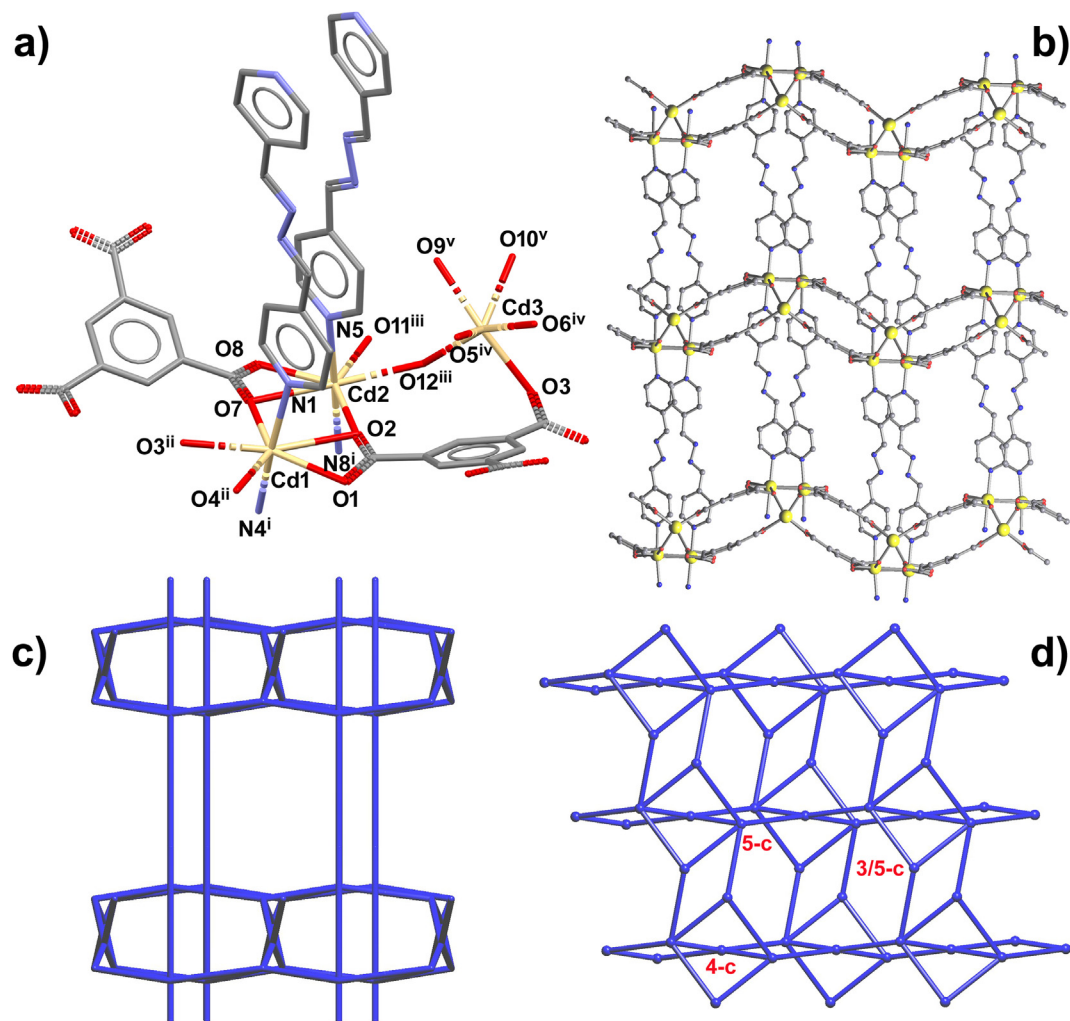


**Fig. 2.** (a) A view of the coordination environment of the three independent cadmium atoms Cd1, Cd2, and Cd3. Superscripts i–v refer to symmetry-related positions described in the footnote of Table S1. (b) View of the 3D pillared framework along the *a* axis. (c) View of the simplified 3D network of **jcr7** topology along the *c* axis and (d) view along the *b* axis showing the simplified 2D thick layer and the position of its nodes of different connectivity.

ligand with respect to the mean plane of the layer (in the pbptz derivative this vector is exactly orthogonal to the layer).

The pillared 3D structure displays free void distributed in channels running along *c*, decorated by the azine groups of the 4-bpdb ligands, corresponding to about 30% of the unit cell volume (Platon [24]). A depiction of the channels is reported in Fig. S2.

The infra-red spectrum of **Cd-MOF** shows characteristic bands of the BTC<sup>3-</sup> ligand in the range 370–1610 cm<sup>-1</sup> (Fig. S3). The bands observed at 1373 and 1435 cm<sup>-1</sup> can be attributed to the symmetric stretching modes of the carboxylate groups; their relative intensity 2:1 is in accordance with the presence in the crystal structure of two chelating-bridging (2.21) carboxylate groups and one chelating (1.11) carboxylate group [23]. The corresponding two asymmetric vibration bands are observed at higher wave number, 1574 and 1615 cm<sup>-1</sup>; their apparent intensity ratio is perturbed by the overlap of the higher energy band with the  $\nu(\text{C}=\text{N})$  stretching bands of the 4-bpdb ligand, which in the free ligand appear at 1594 and 1628 cm<sup>-1</sup>.

### 3.3. Adsorption of organic dyes

The adsorption behavior of the organic dyes Congo Red (**CR**), Neutral Red (**NR**), Methylene Blue (**MB**), and Methyl Orange (**MO**) by the synthesized MOF was investigated. Results indicate that the

MOF shows better adsorptions performance for **CR** and **NR** (Fig. S4). During the adsorption of dye molecules the color of the adsorbent changes from yellow to red for **CR** and **NR**, to blue for **MB** and to orange for **MO**, while the color of the solution fades with time (Fig. S5). Thus **CR** and **NR** dyes were selected for more in depth investigations. The change in the absorption spectra of solutions of **CR** and **NR**, together with the fading of their color following their treatment with the **Cd-MOF** powder (Fig. 3) clearly indicate the removal of the dyes from the solution due to their significant adsorption on the MOF.

#### 3.3.1. Adsorption isotherms

Adsorption isotherms present the relationship between the equilibrium concentration of the dye in solution and the amount of species adsorbed on the adsorbent, at a given temperature. They provide valuable information about the adsorption mechanism that can be employed in designing new adsorbing systems. In this study, data has been analyzed using the most commonly employed adsorption isotherm models (Langmuir, Freundlich, and Temkin equations).

The Langmuir equation describes a system constituted by a homogeneous surface, whose adsorption sites are all energetically identical, onto which the ability of a molecules to bind to a site is

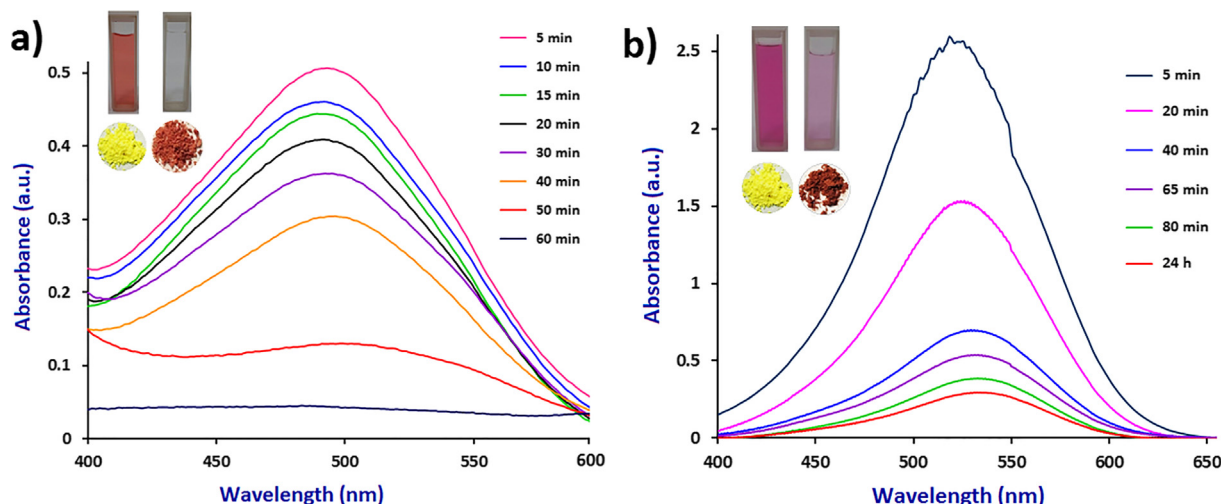


**Fig. 3.** Temporal evolution of the UV-Vis absorption spectra of (a) **CR** and (b) **NR** in water. The photographs show the color of the dye solutions, and of **Cd-MOF** before and after 1 and 24 h of **CR** and **NR** adsorption, respectively.

independent of whether or not nearby sites are occupied [25]. Its expression is:

$$\frac{C_e}{q_e} = \frac{1}{K_L q_m} + \frac{C_e}{q_m}$$

in which  $C_e$  is the equilibrium concentration of the dye on the adsorbent ( $\text{mg L}^{-1}$ ),  $q_e$  is the amount of dye adsorbed per unit mass of adsorbent at the equilibrium concentration ( $\text{mg g}^{-1}$ ),  $q_m$  is the maximum adsorption capacity ( $\text{mg g}^{-1}$ ), and  $K_L$  is Langmuir constant, related to the sorption energy. Values of  $q_m$  and  $K_L$  can be determined from a plot of  $1/q_e$  vs  $1/C_e$ .

The Freundlich equation describes a system constituted by a heterogeneous surface onto which molecules can be adsorbed forming a multilayer [26]. Its linear form is:

$$\log q_e = \log K_F + \frac{1}{n} \log C_e$$

in which  $K_F$  and  $n$  are parameters related to the adsorption capacity and intensity, respectively. Values of  $K_F$  and  $n$  can be determined from a plot of  $\log q_e$  vs  $\log C_e$ .

The Temkin equation assumes that, due to an indirect adsorbate/adsorbent interaction, heat of adsorption decrease linearly with the increase of surface coverage (rather than logarithmically, as implied by the Freundlich equation) [27]. Its expression is:

$$q_e = \frac{RT}{b} \ln K_T + \frac{RT}{b} \ln C_e$$

in which  $K_T$  is the equilibrium binding constant ( $\text{L g}^{-1}$ ) and  $b$  is related to the heat of adsorption ( $\text{J mol}^{-1}$ ). Values of  $K_T$  and  $b$  can be determined from a plot of  $q_e$  vs  $\ln C_e$ .

The isotherm constants and the correlation coefficients were determined for the Langmuir, Freundlich, and Temkin isotherms from a plot of  $1/q_e$  vs  $1/C_e$ , plot of  $\log q_e$  vs  $\log C_e$  and a plot of  $q_e$  vs  $\ln C_e$ , respectively. The results listed in Table 2 indicate that, for both dyes the adsorption process can be described by the Langmuir model ( $R^2$  equal to 0.991 and 0.990 for CR and NR, respectively). In addition, the adsorption of **NR** can also be described, even if with a less accuracy, by the two other models.

### 3.3.2. Adsorption kinetics

Kinetic models of pseudo-first order and pseudo-second order were applied to predict the variation with time of the concentration of the adsorbed dyes. The pseudo-first order model is most widely used for the adsorption of an analyte from aqueous solu-

**Table 2**  
Langmuir, Freundlich, and Temkin isotherms adsorption parameters.

Isotherm model	Parameters	Congo Red ( <b>CR</b> )	Neutral Red ( <b>NR</b> )
Langmuir	$q_m$ (mg/g)	192.3	243.9
	$K_L$ (L/g)	3.71	0.17
	$R^2$	0.991	0.990
Freundlich	$K_F$ [(mg/g)/(mg/L) <sup>1/n</sup> ]	65.11	29.63
	$n$	4.40	1.25
	$R^2$	0.043	0.981
Temkin	$K_T$ (L/g)	30.65	6.97
	$b$ (J/mol)	32.33	31.61
	$R^2$	0.384	0.893

tion. The pseudo-first order kinetic model is given by the Lagergren equation:

$$\log(q_e - q_t) = \log q_e - \frac{k_1 t}{\ln 10}$$

in which  $q_e$  and  $q_t$  are the amounts of dye adsorbed onto the adsorbent ( $\text{mg g}^{-1}$ ) at the equilibrium and at time  $t$ , respectively and  $k_1$  is the first-order rate constant ( $\text{l min}^{-1}$ ) for the adsorption. A plot of  $\log(q_e - q_t)$  vs  $t$  can be used to obtain the rate parameters.

The pseudo-second order kinetics is described by the equation:

$$\frac{t}{q_t} = \frac{1}{k_2 q_e^2} + \frac{t}{q_e}$$

in which  $k_2$  is the second-order rate constant ( $\text{g mg}^{-1} \text{min}^{-1}$ ). A plot of  $t/q_t$  vs  $t$  can be used to obtain the rate parameters. The pseudo-first order and pseudo-second order kinetic models for the adsorption of **CR** and **NR** was investigated using the above equations. Results indicate that the adsorption of **CR** can be fitted by a first-order kinetic model with a correlation coefficient of 0.991 while the adsorption of **NR** can be fitted to a second-order model with a correlation coefficient of 0.990 (Fig. S6).

Various mechanisms have been reported for dye adsorption by MOFs, including anion exchange for ionic MOFs, encapsulation, electrostatic interactions, and also weak interactions, such as H-bond and  $\pi$ - $\pi$  stacking [28,29]. In this work, as clearly indicates by the crystal structure of **Cd-MOF**, the channels' cross section does not allow the entrance of the dye molecules into the framework. On the other hand, due to the overall neutral nature of the structure, ion exchange and encapsulation are not the predominant

mechanisms of adsorption. However,  $\pi$ - $\pi$  stacking interactions between the aromatic rings of  $\text{BTC}^{3-}$  and 4-bpdb and the aromatic rings of **CR** and **NR**, in combination with H-bonds, may be responsible for the adsorption of the dye molecules on the external surface of the **Cd-MOF** particles.

Adsorption of **CR** and **NR** was also investigated by FT-IR spectroscopy (Fig. S3). Due to the superposition of the vibration bands of the loaded dyes with those of the organic linkers constituting the MOF skeleton, it is difficult to precisely assign the observed peaks in the spectra, however the band detected at  $1043\text{ cm}^{-1}$  may be assigned to the  $\nu(\text{S}=\text{O})$  stretching of the sulfonate groups of **CR**.

### 3.4. Synthesis of cadmium-oxide nanoparticles

Cadmium-oxide nanoparticles (CdO NPs) show unique physical and chemical properties and applications in electrochemical devices, information displays, sensor devices, and smart windows.

Size, morphology, and physico-chemical properties of CdO NPs depends on various factors such as: method of preparation, size, morphology, and type of precursors [30]. For these reasons we attempted the preparation of CdO NPs by thermal decomposition of the  $[\text{Cd}_3(\text{BTC})_2(4\text{-bpdb})_2]$  precursor under normal atmospheric pressure at  $500\text{ }^\circ\text{C}$ . During the calcination process, organic components of the 3D framework burn and cadmium oxide nanoparticles

are formed. CdO NPs were characterized by FT-IR spectroscopy, PXRD, particle size analysis, and scanning electron microscopy.

As it is usual for metal-oxide nanoparticles, FT-IR spectrum of the obtained material is simple, due to the release of the organic parts of the 3D architecture (Fig. S3). The peak observed at  $618\text{ cm}^{-1}$  is assigned to the Cd-O bond, while the peaks with weak to medium intensity at  $1660$  and  $3440\text{ cm}^{-1}$  are attributed to the bending and stretching vibrations of the water molecules adsorbed by CdO [31].

The PXRD pattern of the red-brown product confirms the formation of the cubic montepionite structure of CdO (JCPDS No. 05-0640,  $a = 4.6953\text{ \AA}$ ). The sharp and well defined peaks in the PXRD pattern indicate the crystalline nature of CdO NPs; no other impurity peaks were observed in the product (Fig. 4a). SEM images of the particles showed their spherical morphology (Fig. 4b) and a particle size analysis gave an average particle size of  $48\text{ nm}$  with a standard deviation of  $15\text{ nm}$  (Fig. S7).

## 4. Conclusion

A new pillared porous cadmium-organic framework with an uncommon topology has been prepared by means of a mixed-ligand strategy under solvothermal conditions. The topology of the 3D net corresponds to a  $(4\text{-c})(5\text{-c})_2(5\text{-c})_2$ -connected network of type **jc7**. It was found that this MOF could efficiently adsorb organic dyes with an adsorption capacity of  $192.3$  and  $243.9\text{ mg g}^{-1}$  for **CR** and **NR**, respectively. The adsorption process of MOF was well fitted by pseudo-first order and pseudo-second order reaction kinetics for **CR** and **NR** solutions, respectively. Moreover, the MOF can be used as a precursor in a simple preparation of CdO nanoparticles.

## Declaration of Competing Interest

The authors declare that they have no known competing financial interests or personal relationships that could have appeared to influence the work reported in this paper.

## Acknowledgements

The Authors thank Shahid Chamran University of Ahvaz (Grant No.: SCU.SC98.206) and the Università degli Studi di Milano (Piano di Sviluppo di Ateneo, azione B, progetti di interesse interdisciplinare PSR2015-1716FDEMA-07) for financial support. PM and LC thank one of the reviewers for helpful advices about the crystallographic study.

## Appendix A. Supplementary data

CCDC 1902635 contains the supplementary crystallographic data for **Cd-MOF**. These data can be obtained free of charge via <http://www.ccdc.cam.ac.uk/conts/retrieving.html>, or from the Cambridge Crystallographic Data Centre, 12 Union Road, Cambridge CB2 1EZ, UK; fax: (+44) 1223-336-033; or e-mail: [deposit@ccdc.cam.ac.uk](mailto:deposit@ccdc.cam.ac.uk). Supplementary data to this article can be found online at <https://doi.org/10.1016/j.poly.2019.114265>.

## References

- [1] H. Furukawa, K.E. Cordova, M. O'Keeffe, O.M. Yaghi, *Science* 341 (2013) 974–985.
- [2] (a) K.K. Tanabe, Z. Wang, S.M. Cohen, *J. Am. Chem. Soc.* 130 (2008) 8508–8517; (b) K.K. Tanabe, S.M. Cohen, *Chem. Soc. Rev.* 40 (2011) 498–519; (c) P. Deria, J.E. Mondloch, O. Karagiari, W. Bury, J.T. Hupp, O.K. Farha, *Chem. Soc. Rev.* 43 (2014) 5896–5912.

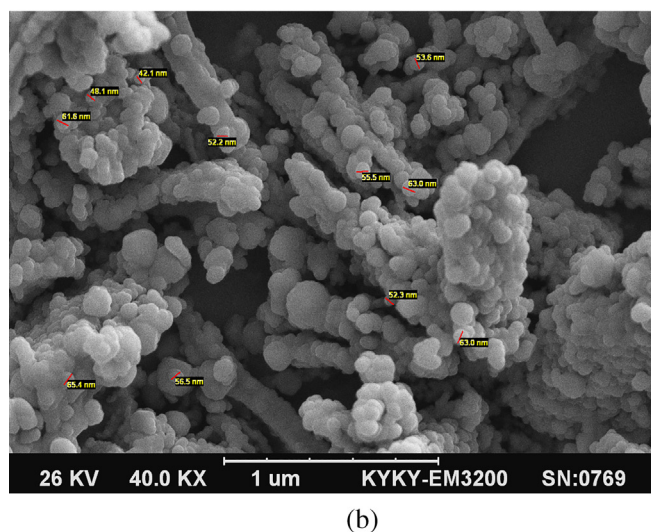
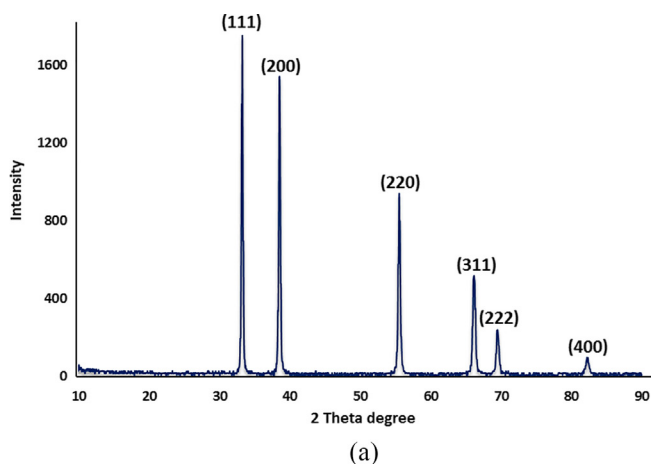


Fig. 4. (a) PXRD pattern of CdO NPs obtained by calcination of **Cd-MOF** in air atmosphere. (b) SEM image of the CdO nanoparticles.

- [3] (a) A.U. Czaja, N. Trukhan, U. Müller, *Chem. Soc. Rev.* 38 (2009) 1284–1293; (b) P. Silva, S.M.F. Vilela, J.P.C. Tomé, F.A. Almeida Paz, *Chem. Soc. Rev.* 44 (2015) 6774–6803.
- [4] (a) S. Parshamoni, S. Sanda, H.S. Jena, S. Konar, *Chem. Asian J.* 10 (2015) 653–660; (b) V. Safarifard, S. Beheshti, A. Morsali, *CrystEngComm* 17 (2015) 1680–1685; (c) H. Ghasempour, A. Azhdari Tehrani, A. Morsali, J. Wang, P.C. Junk, *CrystEngComm* 18 (2016) 2463–2468; (d) B. Bhattacharya, D.K. Maity, R. Mondal, E. Colacio, D. Ghoshal, *Cryst. Growth Des.* 15 (2015) 4427–4437.
- [5] (a) J.L.C. Rowsell, O.M. Yaghi, *Angew. Chem., Int. Ed.* 44 (2005) 4670–4679; (b) R.J. Kuppler, D.J. Timmons, Q.R. Fang, J.R. Li, T.A. Makal, M.D. Young, D. Yuan, D. Zhao, W. Zhuang, H.C. Zhou, *Chem. Soc. Rev.* 253 (2009) 3042–3066; (c) A. Dhakshinamoorthy, A.M. Asiri, H. Garcia, *Chem. Soc. Rev.* 44 (2015) 1922–1947; (d) A.H. Chughtai, N. Ahmad, H.A. Younus, A. Laypkov, F. Verpoort, *Chem. Soc. Rev.* 44 (2015) 6804–6849; (e) P. Horcajada, R. Gref, T. Baati, P.K. Allan, G. Maurin, P. Cuvreur, G. Férey, R. E. Morris, C. Serre, *Chem. Soc. Rev.* 112 (2012) 1232–1268; (f) P.P. Bag, D. Wang, Z. Chen, R. Cao, *Chem. Commun.* 52 (2016) 3669–3672.
- [6] (a) M.Y. Masoomi, A. Morsali, *Coord. Chem. Rev.* 256 (2012) 2921–2943; (b) M. Ramazani, A. Morsali, *Ultrason. Sonochem.* 18 (2011) 1160–1164; (c) K.J. Lee, J.H. Lee, S. Jeoung, H.R. Moon, *Acc. Chem. Res.* 11 (2017) 2684–2692.
- [7] (a) X. Liu, C. Li, S. Han, J. Han, C. Zhou, *Appl. Phys. Lett.* 82 (2003) 1950–1952; (b) T. Krishnakumar, R. Jayaprakash, T. Prakash, D. Sathyaraj, N. Donato, S. Licoccia, M. Latino, A. Stassi, G. Neri, *Nanotechnology* 22 (2011) 325501; (c) N. Rajesh, J.C. Kannan, S.G. Leonardi, G. Neri, T. Krishnakumar, *J. Alloys Compd.* 607 (2014) 54–60; (d) Z. Jia, Y. Tang, L. Luo, B. Li, *Cryst. Growth Des.* 8 (2008) 2116–2120; (e) Z. Guo, M. Li, J. Liu, *Nanotechnology* 19 (2008) 245611.
- [8] (a) R. Das, P. Pachfule, R. Banerjee, P. Poddar, *Nanoscale* 4 (2012) 591–599; (b) C. Jiang, Y. Han, S. Liu, Z. Zhang, *CrystEngComm* 16 (2014) 952–958; (c) K. Anandhan, R.T. Kumar, *Spectrochim. Acta, Part A* 149 (2015) 476–480.
- [9] J. Hu, H. Yu, W. Dai, X. Yan, X. Hu, H. Huang, *RSC Adv.* 4 (2014) 35124–35130.
- [10] (a) I.D. Rattee, *Chem. Soc. Rev.* 1 (1972) 145–162; (b) M. Liang, J. Chen, *Chem. Soc. Rev.* 42 (2013) 3453–3488; (c) W.N. Jones, *Chem. Rev.* 36 (1945) 291–313; (d) M.Q. Doja, *Chem. Rev.* 11 (1932) 273–321.
- [11] (a) Y.C. He, J. Yang, W.Q. Kan, H.M. Zhang, Y.Y. Liu, J.F. Ma, *J. Mater. Chem. A* 3 (2015) 1675–1681; (b) Y.C. Wong, Y.S. Szeto, W.H. Cheung, G. McKay, *Langmuir* 19 (2003) 7888–7894.
- [12] E.M. Dias, C. Petit, *J. Mater. Chem. A* 3 (2015) 22484–22506.
- [13] X. Zhao, X.H. Bu, T. Wu, S.T. Zheng, L. Wang, P.Y. Feng, *Nature* 4 (2013) 2344–2345.
- [14] (a) S.N. Sheng, Y. Han, B. Wang, C. Zhao, F. Yang, M.J. Zhao, Y.B. Xie, J.R. Li, *J. Solid State Chem.* 233 (2016) 143–149; (b) Y. Shen, C.C. Fan, Y.Z. Wei, J. Du, H.B. Zhu, Y. Zhao, *Dalton Trans.* 45 (2016) 10909–10915; (c) P.Y. Du, W. Gu, X. Liu, *CrystEngComm* 18 (2016) 5140–5148.
- [15] (a) E. Amayuelas, A. Fidalgo-Marijuán, B. Bazán, M.K. Urriaga, G. Barandika, M. I. Arriortua, *CrystEngComm* 18 (2016) 1709–1712; (b) M.Y. Masoomi, M. Bagheri, A. Morsali, *Ultrason. Sonochem.* 33 (2016) 54–60; (c) X.X. Wang, Z.X. Li, B. Yu, K.V. Hecke, G.H. Cui, *Inorg. Chem. Commun.* 54 (2015) 9–11; (d) W.H. Huang, J.Z. Li, L. Sha Gao, Y.X. Wang, S.Y. Liu, M. Jiang, T. Liu, Y.Y. Wang, *Dalton Trans.* 45 (2016) 15060–15066; (e) A. Abbasi, M. Soleimani, M. Najafi, S. Geranmayeh, *Inorg. Chim. Acta* 439 (2016) 18–23; (f) M.Y. Masoomi, A. Morsali, P.C. Junk, *CrystEngComm* 17 (2015) 686–692.
- [16] Z. Hasan, S.H. Jhung, *J. Hazard. Mater.* 283 (2015) 329–339.
- [17] Mercury 3.0, Cambridge Crystallographic Data Centre, Cambridge, 2018.
- [18] V.A. Blatov, A.P. Shevchenko, D.M. Proserpio, *Cryst. Growth Des.* 14 (2014) 3576–3586.
- [19] D.M. Ciurtin, Y.B. Dong, M.D. Smith, T. Barclay, H.C. zur Loye, *Inorg. Chem.* 40 (2001) 2825–2834.
- [20] Bruker, CELL\_NOW 2008/4, TWINABS 2012/1, and SHELX 2014/7, Bruker AXS Inc., Madison, Wisconsin, USA.
- [21] B. Bhattacharya, R. Haldar, D.K. Maity, T.K. Maji, D. Ghoshal, *CrystEngComm* 17 (2015) 3478–3486.
- [22] (a) S. Parshamoni, S. Sanda, H.S. Jena, K. Tomar, S. Konar, *Cryst. Growth Des.* 14 (2014) 2022–2033; (b) R.A. Coxall, S.G. Harris, D.K. Henderson, S. Parsons, P.A. Tasker, R.E.P. Winpenny, *J. Chem. Soc., Dalton Trans.* (2000) 2349–2356; (c) S. Khatua, S. Goswami, S. Parshamoni, H.S. Jena, S. Konar, *RSC Adv.* 3 (2013) 25237–25242.
- [23] J.M. Seco, S. Pérez-Yáñez, D. Briones, J.Á. García, J. Cepeda, A. Rodríguez-Diéguez, *Cryst. Growth Des.* 17 (2017) 3893–3906.
- [24] A.L. Spek, *J. Appl. Crystallogr.* 36 (2003) 7–13.
- [25] I. Langmuir, *J. Am. Chem. Soc.* 40 (1918) 1361–1403.
- [26] H. Freundlich, *J. Phys. Chem.* 57 (1906) 1100–1107.
- [27] M.I. Tempkin, V. Pyzhev, *Acta Phys. Chim. USSR* 12 (1940) 327–356.
- [28] K.-Y.A. Lin, H.-A. Chang, *Chemosphere* 139 (2015) 624–631.
- [29] H. Normohamadi, M. Fat'hi, M. Ghaedi, S. Azizzadeh, V. Nobakht, *J. Mol. Liq.* 262 (2018) 71–77.
- [30] M.Y. Masoomi, A. Morsali, *Coord. Chem. Rev.* 256 (2012) 2921–2943.
- [31] (a) K. Anandhan, R. Thilak Kumar, *Spectrochim. Acta A* 149 (2015) 476–480; (b) S. Sivakumar, A. Venkatesan, P. Soundhirarajan, C.P. Khatiwada, *Spectrochim. Acta A* 151 (2015) 760–772; (c) J.R. Ferraro, *Low-Frequency Vibrations of Inorganic and Coordination Compounds*, Plenum Press, New York NY, 1971.